Influence of strain rate on strength and deformation of granular material: a DEM based study

Sagar Biswas[1,*], *Vivek* Padmanabha[1]

[1] Department of Civil Engineering, Indian Institute of Technology Guwahati, India

Abstract. Granular materials are subjected to compressive loading in various scenarios, including ceramic pebble beds in fusion reactors, packed granular beds in chemical reactors, sand beneath structural foundations and dams, ballast in railway tracks, and food grain storage in silos. Granular materials behave differently under varying strain rates, influenced by particle shape, size, friction, cohesion, roughness, elasticity, and coefficient of restitution. This study uses three-dimensional Discrete Element Method (DEM) tool LIGGGHTS to investigate the effect of strain rate, ranging from quasi-static to dynamic loading, in uniaxial compression mode. A progressive replacement breakage criterion is applied to particles that exceed the critical stress during simulation, based on an energy threshold, following Weibull distribution for fragment generation. This study establishes a comprehensive correlation between micro and macro phenomena. Particle-level properties such as contact force, acceleration, particle breakage, rearrangement affect the macro-scale phenomena such as stress-strain response, peak strength, and failure modes. The findings reveal that strain rate variations significantly impact the breakage behavior of particles. This study provides valuable insights into the strain rate dependence of granular material behavior, contributing to a deeper understanding of their mechanical performance under varying loading conditions.

1 Introduction

In the realm of granular material research, the DEM has been extensively used to simulate and understand different material behaviors under compressive loading. For instance, DEM is used to investigate the effect of particle size reduction of granular materials[1], focusing on the evolution of particle breakage in uniaxial compression tests. The failure mechanisms of porous granular materials are explored [2], and the behavior of cemented granular materials is examined [3]. Additionally, DEM is employed to study the scaling effects in both cohesionless and cohesive solids [4]. These studies highlight the versatility and importance of DEM in understanding granular material behavior across various applications, helping to minimize experimental hardships.

Granular materials can undergo breakage under increasing strain rates in uniaxial compression test. Several studies have been conducted to accurately model the breakage of a parent particle by introducing two symmetrically sized daughter particles [5,6], three symmetric daughter particles [7] , three different sized particles, four different-sized particles [8], random-sized particles [9]. Particle breakage is normally encountered by two processes: first, particle replacement method when the particle's internal peak stress exceeds a critical stress threshold; second, the agglomerate method.

*Corresponding author: b.sagar@iitg.ac.in

In the agglomerate method, bonded particles are generated upon breakage considering bonding parameters, sub-particle size, complex shape and interaction forces, which require intensive computational accuracy. In contrast, particle replacement method has relatively low computational load during the initial breakage stages, but the computational load increases enormously as the simulation progresses[10].

Recent studies have confirmed that strain rate influences the particle breakage significantly, when potential of grain fragmentation is high due to excessive confinement pressure. The uniaxial compression test is best suited for providing intense confinement and progressive loading conditions to analyse particle breakage, Whereas DEM is best suited to analyse micromechanical properties such as fabric tensor, co-ordination number to bridge micro-macro mechanical behaviour of granular assembly[11]. However, limited studies have focused explicitly on the rate dependent particle breakage subjected to uniaxial compression loading. In the present study particle replacement method is applied to capture breakage condition under high strain rate loading in uniaxial compression test.

2 Methodology

The uniaxial compression simulation is conducted in a cylindrical frame, where a downward-moving top plate applies increasing mechanical load, causing deformation of the glass bead bed. Uniaxial

compression tests (UCTs) are carried out on glass beads over a range of strain rates from quasi-static to dynamic loading conditions, using the 3D Discrete Element Method tool LIGGGHTS.

2.1. Validation

To validate the methodology, numerical simulation is compared in Fig.1 with results for Li_4SiO_4 pebble bed subjected to uniaxial compression loading in a square simulation box with constant rate of 0.5 mm/s [12]. Slight discrepancy can be observed here due to initial packing differences of particles in the simulation box and also due to different simulation tools. The simulation is initialized with 4000 spherical particles of 1 mm diameter, packed in a box of dimensions 15 mm × 15 mm × 15.2 mm. Each particle has a density of 2390 kg/m³, Young's modulus of 90 GPa, Poisson's ratio of 0.24, and a static coefficient of friction of 0.1.

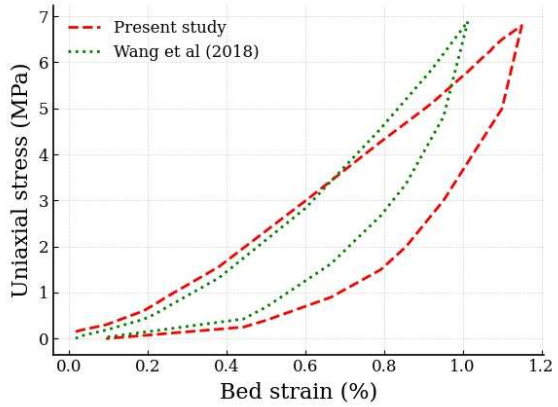

Fig. 1. Validation graph of uniaxial stress vs. bed strain under uniaxial compression, comparing the present simulation results with numerical data on Li_4SiO_4 pebbles used in nuclear reactors [12].

2.2. Modelling parameters

A one-dimensional compression test is conducted on granular glass beads with a diameter of 2.4 mm inside a cylindrical box with a diameter of 28.7 mm. Initially, the box is filled with 1,713 particles, reaching a nominal height of 38.185 mm, as illustrated in Fig.2. During particle generation, overlaps may occur, resulting in excessive particle-particle and particle-wall contact forces. However, particle breakage is prevented during the generation and filling process in the simulation.

To minimise errors in the initial compressed bed height relative to the particle count, a uniform relative density of 1.966 g/cc is maintained within the simulation domain by adjusting the top plate position and fixed number of particles within the domain. The glass bead's material properties are assigned to the simulation including a Young's modulus of 70 GPa, Poisson's ratio of 0.22, and density of 2,390 kg/m³. A static friction coefficient of 0.1 is applied for both bead-bead and bead-wall interactions, along with a coefficient of restitution of 0.8. Gravity, at 9.81 m/s², is consistently applied throughout the simulation to settle the particle in simulation box and achieve a stable glass beads assembly.

2.3. Breakage criteria

Particle internal strain energy is given by [13],

$$E = \int_0^{\Delta_c} F\delta\Delta \quad (1)$$

Where Δ is the particle deformation; Δ_c is the deformation at fracture and δ is the normal overlap. Normal damping force can be calculated as [14],

$$F = \frac{4}{3}E^*\sqrt{R^*}\delta^{3/2} \quad (2)$$

$$R^* = \frac{R_i + R_j}{R_i * R_j} \quad (3)$$

$$\frac{1}{E^*} = \frac{1-\mu_i^2}{E_i} + \frac{1-\mu_i^2}{E_j} \quad (4)$$

Where E_i, μ_i, R_i and E_j, μ_j, R_j represents Young's modulus, Poisson's ratio and radius of particle i and j respectively.

Weibull Probability P_B of the fracture of the chain which consist of z links of strength σ_s strength when the load is applied and m is a free probability distribution parameter.

$$P_B = 1 - \exp\left\{-z\left(\frac{\sigma}{\sigma_s}\right)^m\right\} \quad (5)$$

A particle deforms elastically when collision forces initially act on it, absorbing impact energy as elastic strain energy. According to the Griffith criterion, internal stress within the particle increases until critical threshold stress with its most sensitive flaw. This critical stress level is influenced by the mass specific threshold energy $W_{m,\ min}$ to further damage the particle. Fracture begins at the weakest flaw once the accumulated stress exceeds this threshold. When the probability of breakage P is sufficiently high, particle breakage will occur[13]. Vogel and Peukert introduced a probability function P, based on similarity of breakage of particle of similar shape and mechanical fracture model[15].

$$P = 1 - \exp\left[-f_{Mat}dk(W_m - W_{m,\min})\right] \quad (6)$$

Where $W_{m,\ min}$ is the mass specific threshold energy which a particle can absorb without breakage, k is the number of stress events with a constant mass specific impact energy W_m, f_{Mat} is a material parameter speicifying the resistance against fracture and d is the particle diameter. For DEM application, Probability function of breakage modified by considering different specific impact energies E_i are of interest[16].

$$P = 1 - \exp[-f_{Mat}d\sum_i(E_i - E_0)] \quad (7)$$

In experiments E_0 is defined by the energy at which probability of breakage in below 5% for infinite no of tests. By validating the m value equal to 4 Vogel and Peukert [17] have validated the value of f_{Mat} & $dW_{m,\min}$ for breakage for glass beads as 0.944 Kg/Jm and $dW_{m,\min}$ as 0.297 Jm/Kg by.

3 Result

Three strain rate cases (155 s^{-1}, 310 s^{-1} & 424 s^{-1}), representative of blast & impact loading conditions, were considered to investigate the mechanical behaviour and breakage patterns of glass beads under uniaxial compression. As shown in the fig. 3, the uniaxial compressive stress calculated from reaction forces obtained from top and bottom plate of the cylindrical box, increases with strain rate & corresponding loading rate slight linearly. Breakage occurs in particle when internal strain energy of particle surpasses the Griffith's energy threshold. At this stage disturbance can be observed due to single particle deletion and multiple particle formation within a single step. At lower strain rate & loading rates, particle breakage takes place at higher bed strain, whereas at higher strain rate and loading rate, early bed strain breakage occurred. Strain rate & Beds strain (%) are calculated as follows:

$$\text{Strain rate} = \frac{\text{Top plate velocity in negative z direction}}{\text{Height of the no compression glass bed}} \quad (8)$$

$$\text{Bed strain (\%)} = \frac{\text{Height of the no compression glass bed} - \text{Compressed glass bed height}}{\text{Height of the no compression glass bed}} \quad (9)$$

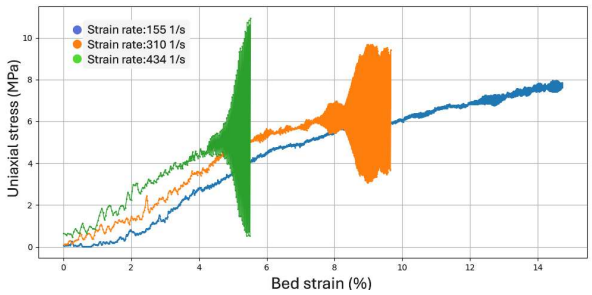

Fig. 2. Graph of stress vs strain corresponding to three strain rate & corresponding loading rate under uniaxial compression test for granular beads.

Particle breakage occurs when the internal strain energy exceeds the Griffith's energy threshold, progressing successively in accordance to the t_n family approach, where mass fraction of the progeny particles is defined based on the parent particle size for mass conservation. The fracture of the particles occurs through transformation of energy and momentum by triggering the weakest flaw into crack; consequently, the momentum of the fragments after breakage is smaller than initial momentum of the parent particle. Initial breakage takes place at the topmost layer and gradually propagates to the lower layer as can be seen in Fig. 3. This behaviour results from sudden stress accumulation followed by gradual release. Simulation stops due to excessive neighbour counts within defined domain volume when the bed is overly compressed. Comparative higher strain rate lead to increased fragmentation at the top layer with finer particle size distribution.

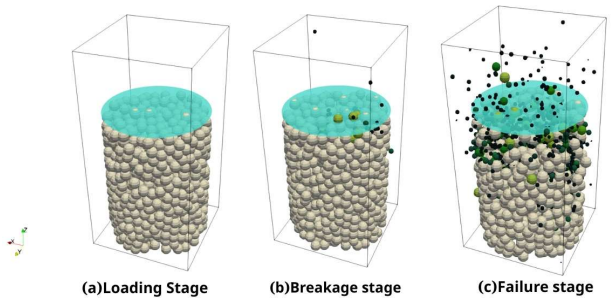

Fig. 3. (a)Loading stage, (b)breakage stage & (c)Failure stage of simulation under uniaxial compression test for granular beads subjected to strain rate of 310 s^{-1}.

There is a strong co-relation between strain rate (s^{-1}) and uniaxial stress as illustrated in Fig. 4. The increase in the uniaxial stress corresponds with higher strain rate due to re-arrangement and breakage of particle. At higher strain rate, particle get insufficient time to transfer massive energy which results in fragmentation with finer particle size distribution through multiple flaw propagation. This demonstrates that the dynamic property of granular material like peak stress have strong influence on loading condition specially in the high strain rate range.

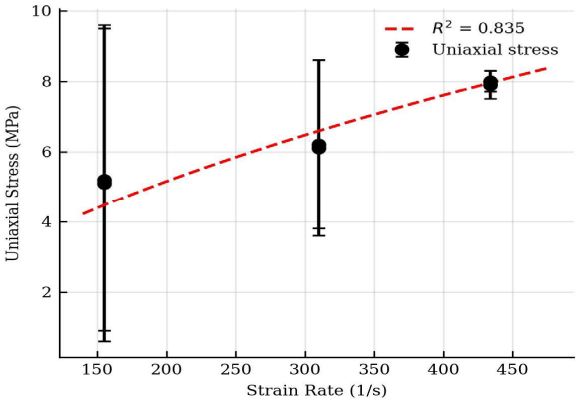

Fig. 4. Graph of strain rate vs uniaxial stress under uniaxial compression test.

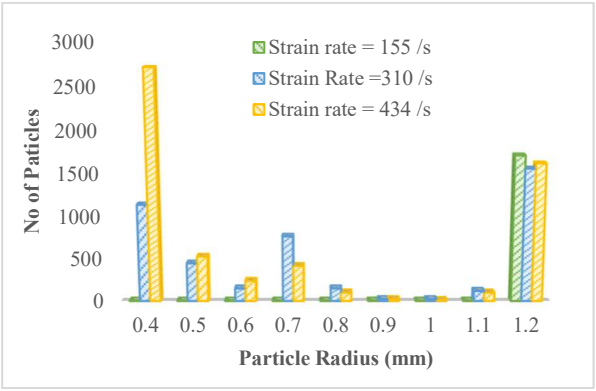

Fig. 5. Fragments size distribution at failure corresponding to three loading condition under uniaxial compression test.

Number of fragments (progeny particle) increases with increasing strain rate at failure due to rapid and excessive stress accumulation, indicating widespread fracture propagation, as shown in fig. 5. At the highest strain rate (424 s^{-1}), the fragment size distribution shifts

towards smaller radius indicating more extensive fragmentation compared to lowest (155 s^{-1}) strain rate. An interesting observation can be made at the lowest strain rate, where only one particle breakage takes place. Whereas in other two higher strain rate cases (310 s^{-1} & 434 s^{-1}), 96 and 152 mother particle experienced breakage. At the higher strain rate, reduced stress relaxation time within particle & rapid particle deformation leads to particle breakage, as particle experience high kinetic energy. At higher deformation rate, force chains form and collapse rapidly and abruptly whereas continuous steady force chains formulate in lower strain rate loading.

4 Conclusion

- A strong co-relation between varying strain rate and stress accumulation can be observed under uniaxial loading of granular glass beads.
- Uniaxial compressive stress increases with strain rate until failure, indicating a rate dependent mechanical behaviour.
- The fragment size distribution is strongly influenced by the applied strain rate/ loading rate with higher strain rate leading to propagation of finer fragments size, due to rapid energy accumulation. Maximum particle distribution can be observed at minimum specified radius.

5 Reference

1. C. Zhang, Y. Chen, Y. Wang, Q. Bai, Green Smart Min. Eng. **1**, 190 (2024).
2. F. Kun, I. Varga, S. Lennartz-Sassinek, I.G. Main, Phys. Rev. E **88**, 062207 (2013).
3. Y. Yamaguchi, S. Biswas, T. Hatano, L. Goehring, Phys. Rev. E **102**, 052903 (2020).
4. S.C. Thakur, J.Y. Ooi, H. Ahmadian, Powder Technol. **293**, 130 (2016).
5. J.P. de Bono, G.R. McDowell, Comput. Geotech. **78**, 11 (2016).
6. G.R. McDowell, J.P. de Bono, Géotechnique **63**, 895 (2013).
7. W. Zhou, L. Yang, G. Ma, X. Chang, Y. Cheng, D. Li, Granul. Matter **17**, 497 (2015).
8. W. Zhou, L. Yang, G. Ma, X. Chang, Z. Lai, K. Xu, Granul. Matter **18** (2016).
9. J. Bruchmüller, B.G.M. van Wachem, S. Gu, K.H. Luo, Powder Technol. **208**, 731 (2011).
10. S.K. Das, H. Abuel-Naga, Minerals **14**, 1102 (2024).
11. S. Wang, S. Wang, Q. Xu, H. Chen, Fusion Eng. Des. **128**, 53 (2018).
12. L.M. Tavares, R.P. King, Int. J. Miner. Process. **54**, 1 (1998).
13. M. Manokaran, M. Morgeneyer, Granul. Matter **10**, 304 (2008).
14. L. Vogel, W. Peukert, Int. J. Miner. Process. **74** (2004).
15. R.D. Morrison, F. Shi, R. Whyte, Miner. Eng. **20**, 303 (2007).
16. L. Vogel, W. Peukert, Chem. Eng. Sci. **60**, 5164 (2005).